New radial turbine dynamic modelling in a low-temperature adiabatic Compressed Air Energy Storage system discharging process

Wei He [a], Jihong Wang [a, b, 1], Yulong Ding [c]

[a] School of Engineering, University of Warwick, Coventry, United Kingdom, CV4 7AL, United Kingdom

[b] School of Electrical & Electronic Engineering, Huazhong University of Science & Technology, China

[c] Birmingham Centre for Energy Storage, School of Chemical Engineering, University of Birmingham, Birmingham B15 2TT, United Kingdom

Abstract:

It is challenging to gain insight of a Compressed Air Energy Storage (CAES) system dynamic behaviour under various operation conditions due to its complexity with mixed mechanical, thermal, chemical and electrical processes in one. Although a number of studies are reported on CAES steady state and dynamic modelling to reveal its characteristics, few studies have been reported in whole CAES system dynamic modelling involving a radial turbine. This paper explores a new method to analyse the transient performance of radial turbines while it is integrated with whole low temperature Adiabatic-CAES system. The proposed modelling method approximates the average air flow within single stator/rotor stage. By applying the principle of energy and torque balance on the transmission shaft, the dynamic speed-torque characteristics of the turbine is obtained with a "quasi dynamic iterative searching" process. The model is then integrated to a simulation platform, which is created to synchronise the wide range of time scale dynamic responses including heat transfer, mechanical and electrical energy conversion processes. As every component of the low temperature adiabatic CAES system is built on its fundamental physical and engineering principles, the model is capable of revealing the system transient characteristics. Based on the model, various simulation studies are conducted and the results are compared with the operation data. It provides a valuable tool for preliminary design of a radial turbine to test its suitability in full and partial load operation conditions and its transient behaviours.

Keywords:

Adiabatic Compressed Air Energy Storage, Radial turbine, Dynamic Modelling, Fluctuated demand

[1] Corresponding author: Tel: +44 (0)24 765 23780 (J Wang)
E-mail address: Jihong.wang@warwick.ac.uk

1. Introduction

Energy storage recently attracts great attentions in addressing the issues associated with rapid growth of power generation from intermittent renewable energy sources. Among various technologies for electrical energy storage, Compressed Air Energy Storage (CAES) is one of two proven technologies suitable for building large-scale plants (over 100 MW). There are two successfully operated CAES plants in the world. The first utility-scale CAES is the 290 MW Huntorf plant in Germany using salt dome for air storage, which was built in 1978. The other is an 110 MW plant with a capacity of 26 hours in McIntosh, Alabama, USA. The common feature of the two CAES plants is that they both require fossil fuels to achieve its rated power. To avoid consuming the fossil fuels, adiabatic CAES (A-CAES) with Thermal Energy Storage (TES) become a new technology development direction.

Wolf and Budt proposed a low-temperature A-CAES (LTA-CAES) using multi-stage radial compressors and expanders, in which operational temperature of heat storage was between 95-200 ^{o}C [1]. According to their analysis, advantages of the LTA-CAES include the fast start-up characteristics, wide-ranging part load, highly available thermal working fluid, low pressure drop of compressed air and potential plant profitability [1]. Luo et al also studied a LTA-CAES system and indicated the cycle efficiency and heat energy recycle efficiency can reach around 68% and 60%, respectively [2]. With the acceptable cycle efficiency, potential operational flexibility of the LTA-CAES plant makes it a promising and feasible solution. But recently, Wang et al presented the first public experiment on a LTA-CAES system [3]. Although the feasibility of the LTA-CAES was demonstrated in practice, only an averaged cycle efficiency of 22.6% was achieved in the pilot "TICC-500" plant [3]. The low efficiency was mainly caused by nature of the transient system operation of the A-CAES system in realistic operations, which reduced the efficiency of components when they were operated from their design conditions.

From the published literature, previous investigations developed dynamic analysis of CAES systems with volume-based expanders. Sun et al. developed a complete dynamic mathematical model of a hybrid CAES-wind turbine system, in which scroll expander is selected for storing the compressed air [4]. Krupke et al further demonstrated the benefits of improved efficiency and flexibility brought to the wind turbine by the hybridization with the scroll expander based CAES system to smooth the time variant fluctuations [5]. Compared to the volume-based expanders, prior studies about the turbine-based CAES system mainly focused on steady-state thermodynamic analysis. Liu and Wang thermodynamically analysed a modified A-CAES system using steady-state mathematical models, and found 3% exergy efficiency increase [6]. Yao et al searched for the Pareto front of a small-scale CAES system between thermodynamic and economic performance [7]. Guo et al proposed a CAES system integrated with ejector and indicated a 3.41% efficiency increase by thermodynamic analysis [8]. Particularly, the radial turbine is recognised for high efficiency and light weight in high power capacity compared to volume based expanders. The power rating of a radial turbine is usually up to several megawatts [9], and thus, it has great potential in small-scale and medium-scale CAES systems. But the radial turbines usually have low efficiency in off-design operations [10]. As a consequence, evaluating the off-design operations' performance and the transitions of the CAES system with the radial turbine become particularly important due to the varied performance of the radial turbine and complex interactions between the component and system.

However, there are very limited studies that addressed the dynamic characteristics of turbines. Arabkoohsar et al. considered the off-design performance of compressors/turbines using an empirical relation in the steady-state thermodynamic modelling [11]. Wolf dynamically simulated a high-temperature A-CAES system in which main system response was dominated by the heat storage and turbines were modelled using empirical polynomial models [12]. Similarly, Sciacovelli et al.

investigated how packed bed heat storage dynamics inducing off-design conditions of turbines [13], but mechanical responses of turbines were not resolved. Li et al. only corrected the mass flow rate of the air turbine under off-design conditions in an integrated system of a diesel genset and a CAES unit [14]. Zhao et al. selected two operational modes of the CAES system and carried out the off-design operational analysis in different power levels and speed levels [15], in which each operation (100% load or partial load) was considered as the static operation. Briola et al. used the experimental characteristic curves as the basis and predicted the operative behaviour of turbomachines over a wider range of conditions by the affine transformation method [16].

The complexity of turbine-generator rig dynamics is resulted from the multiple conversions between air momentum/potentials, mechanical and electrical energy. Therefore, a new "quasi dynamic iterative searching" method for modelling turbine dynamic behaviours is proposed in this study, aiming to understand the dynamic characteristics of turbines in a LTA-CAES operation cycle. The turbine dynamic changes is derived in response to the mechanical shaft dynamics which the turbine is connected to and the mechanical-electrical energy conversion happens through, by decoupling the air mass and momentum inside the turbine flow path as purely flow resistive [17]. This shaft dynamic response repeats every numerical step iteratively. The mean-line model is adopted to generate the characteristic equations of the turbine which are used for iterative searching of the balance states to match the shaft dynamic variations at every time-step. This model is built on the detailed knowledge of the turbines' geometry, e.g. size of stator/rotor, to generate the characteristic curves of turbomachinery in various operational loads.

Furthermore, the LTA-CAES system has highly dynamic coupling in between components and wide variations of component dynamic response time scales. It is crucial to have simulation models accurate enough for main components. With these models, the assembled whole system model can reveal the system dynamic responses under various operation conditions and parameters. Therefore, this study starts from the key component (radial turbines) modelling and verification to the whole LTA-CAES system with integration of the turbines. A new "quasi dynamic iterative searching" method is proposed to reflect both the off-design operative behaviours and dynamic characteristics of the radial turbine in the LTA-CAES system. In addition to the radial turbines, the associated component models are also introduced which include heat exchanger (HEX), air storage, sensible thermal storage, and generator. The feasibility of the dynamic modelling methodology is investigated by comparing the simulation results with the published experimental data. Then, with the validated modelling method, effects of HEX's design are evaluated, and a case study is presented in the paper to reveal the start-up and operation transitions of the LTA-CAES system and radial turbines between design and off-design operations.

2. System configuration: discharge process of the low temperature Adiabatic Compressed Air Energy Storage

The system configuration considered in this study utilises the latest pilot A-CAES plant named "TICC-500", which is built by the Key Laboratory of Cryogenics, Chinese Academy of Science [3]. The maximum output power of the generator is designed to be 500 kW. The pilot plant has five compression stages with inter-cooling and three expansion stages with inter-heating. The TES system employs pressurised water as the thermal fluid. Particularly in the discharge period, as shown in Fig. 1, pressurised water from the hot water tank heats up compressed air from the air storage tank in the HEX before the air flowing into the turbine stages. Then, energy from the reheated compressed air is converted to the mechanical energy of the rotating turbines. The cooled water flows to the cold water tank which stores the cold for cooling down the compressed air during the charge period. Additionally, a throttle valve is placed before the HEX in the first stage to regulate the inlet pressure according to

the design operation. A single shaft connects all the three stage turbines, which drives the generator through the gear box.

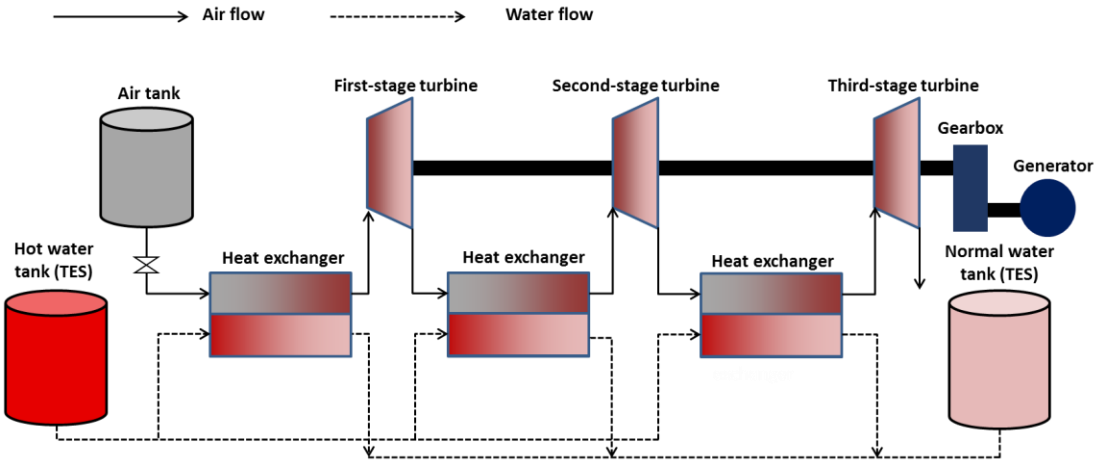

Figure 1 Schematic diagram of the studied LTA-CAES discharge system

3. Mathematical models of the associated system components

This section introduces the mathematical models of the major components associated with the LTA-CAES system. These models predict the performance of the components considering their basic geometric parameters.

3.1. Radial turbine

In a radial turbine, energy conversion can be approximately described by the Euler Equation of Turbomachines [18]. Different geometries and fluid conditions significantly affect the performance of the turbine. In an inflow radial (IFR) turbine used in CAES, compressed air enters the turbine stator/rotor at the outer radius with one velocity and leaves at the inner radius with another velocity. Fig. 2 illustrates the velocity triangles of air at inlet and outlet of stator and rotor. Fig. 2(a) shows the velocity triangles in the design operation and those in the off-design operations are illustrated in Fig. 2(b). In the design operation, air flows into the rotor according to the designed inlet angle. In contrast, in the off-design operations, the mismatch occurs between the flow angle and the designed inlet angle, leading to energy losses. The turbine is regarded as a purely resistive fluid flow component in which the accumulations of mass, momentum and energy inside the turbine flow path are negligible [17]. Therefore, average air flow in the stator/rotor without the unsteadiness of internal flow is considered in the IFR modelling. The “quasi dynamic” speed-torque characteristics of the radial turbine is modelled through the mechanical transmission of turbine-generator rig.

In the modelling of the radial turbine, the considered losses of air flow energy include: 1) frictional losses in both the stator and the rotor. The fractional losses are incurred by the velocity gradient layers within the air flow due to the viscosity. Air flows in both the design and off-design operations have fractional losses; and 2) incidence losses due to the non-zero effective angle of incidence in the off-design operations. A non-zero incidence angle can arise from variations in the rotating speed, the flow rate, and the flow angle due to the changed inlet guide vane [19]. If the relative flow inlet angle of the rotor is less than the designed relative flow angle, a separation zone could be formed on the front of the suction surface and gradually move to the outlet of the rotor. In contrast, if the relative flow inlet angle is larger than the designed relative flow angle, the separation zone occurs on the front of the pressure surface.

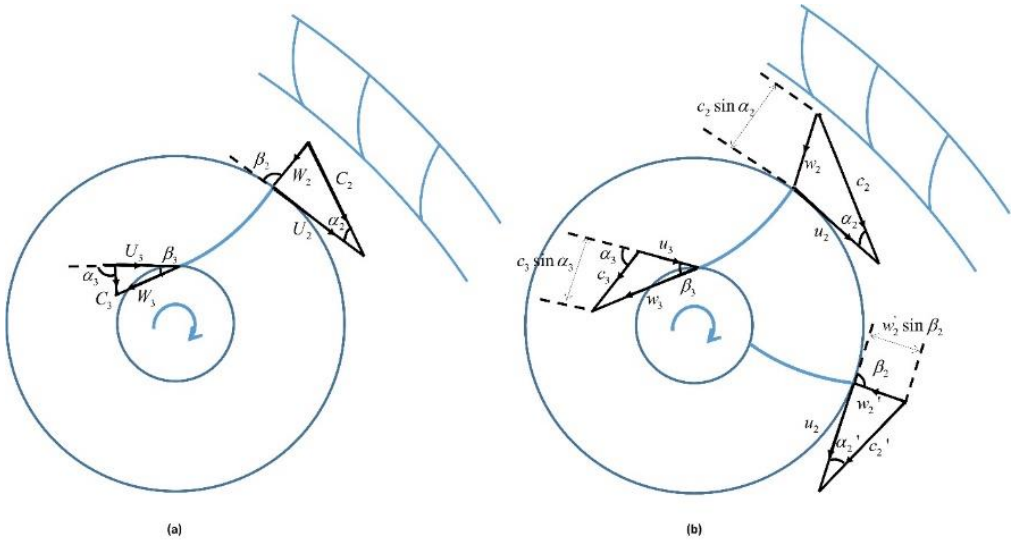

Figure 2 Schematic velocity triangles at inlet and outlet of the rotor.

The changes in the momentum of the air result in the work released by the turbine, which drives the externally applied torque, namely a generator in the A-CAES. The specific work can be described as follows,

$$w_t = \Delta h = u_2 c_{w2} - u_3 c_{w3} \tag{1}$$

where u and c_w are the tangential velocity of the rotor and air, respectively. When a 90 degree IFR turbine is considered at its nominal design condition, it leads to $c_{w3} = 0$ and $c_{w2} = u_2$. Furthermore, the tangential velocity of the rotor is dependent on the rotor size and the rotation speed, which is

$$u_2 = \frac{\pi N D_2}{60} \tag{2}$$

where D is diameter of the rotor, N is rotational speed in rpm. The velocity of air at the inlet of the rotor is converted from the pressure drop of the compressed air in the stator. Velocity of the air at the outlet of the stator can be approximated by assuming adiabatic air flow in an equivalent nozzle with energy loss,

$$c_2 = \sqrt{2(\Delta h_{1-2s} - \Delta h_{2loss})} = \sqrt{2(\frac{\kappa}{\kappa - 1} R\, T_1 [1 - (\frac{p_2}{p_1})^{\frac{\kappa-1}{\kappa}}] - \Delta h_{2loss})} \tag{3}$$

where c is absolute velocity, p is pressure, R is gas constant, T is temperature, κ is isentropic index, and Δh_{2loss} is enthalpy loss due to passage friction in the stator. Subscript 1 and 2 denote the inlet and outlet of the stator. Energy loss in the stator can be approximated by [19],

$$\Delta h_{2loss} = \frac{1}{2} \xi_2 c_2^2 \tag{4}$$

in which ξ_2 is enthalpy loss coefficient of the stator.

As shown in Fig. 2(b), part-load operation results in the incidence losses due to the sudden change of the flow direction which leads to flow separation. Wallace proposed a simplified method to estimate this incidence loss in off-design operations based on energy conservation [20].

In the off-design operation, a sudden change of the flow direction formats shock, which is the dissipation of the kinetic energy. Based on the assumed constant pressure from exit of the stator and inlet of the rotor, equations of mass and energy conservation can be derived. The energy balance becomes [20]

$$c_p T_2 + \frac{c_2^{\ 2}}{2} = c_p T_2^{'} + \frac{c_2^{'2}}{2} + [c_2 \cos\alpha_2 - c_2 \sin\alpha_2 \frac{T_2^{'}}{T_2} \cot\beta_2 - u_2]u_2 \tag{5}$$

where $T_2^{'}$ and $c_2^{'}$ are the varied temperature and velocity due to the sudden deflection of the flow, c_p is specific heat capacity. α_2 is rotor absolute inlet angle. β_2 is rotor relative inlet angle. The equation of continuity in radial direction is [20]

$$\frac{w_2^{'} \sin\beta_2}{c_2 \sin\alpha_2} = \frac{T_2^{'}}{T_2} \tag{6}$$

where $w^{'}$ is the varied relative velocity. Based on Equations (5) and (6), the changed temperature $T_2^{'}$ due to the incidence loss can be obtained. Furthermore, the relative velocity of the air at the outlet of the rotor is,

$$w_3^{\ 2} = w_2^{\ 2} + 2(\Delta h_{2-3s} - \Delta h_{3loss}) + u_3^{\ 2} - u_2^{\ 2} \tag{7}$$

where $\Delta h_{3loss} = \xi_3 w_3^2 / 2$ is enthalpy loss due to passage friction in the rotor [19]. Subscript 3 denotes the outlet of the rotor. Therefore, considering all energy losses, the torque produced in the rotor can be obtained. The torque is composed of two parts, namely, one is caused by the suddenly deflected flow when entering the rotor, and the other one is produced within the rotor passage. Therefore, the two torques can be expressed as [20]

$$\tau_s = \frac{[c_2 \cos\alpha_2 - c_2 \sin\alpha_2 \frac{T_2^{'}}{T_2} \cot\beta_2 - u_2]D_2}{2}; \tau_r = \frac{[c_2^{'} \cos\alpha_2^{'} + \frac{D_3}{D_2} c_3 \cos\alpha_3]D_2}{2} \tag{8}$$

where τ_s is the torque due to flow deflection and τ_r is the mechanical torque of the rotor. Accordingly, the isentropic efficiency of the turbine is

$$\eta_s = \frac{(\tau_s + \tau_r)\omega}{\Delta h_{13s}} = \frac{(\tau_s + \tau_r)}{\frac{\kappa}{\kappa - 1} R\, T_1 [(\frac{p_3}{p_1})^{\frac{\kappa-1}{\kappa}} - 1]} \frac{2\pi N}{60} \tag{9}$$

where ω is the rotation speed of turbine in rad/s.

Simulation needs to find an appropriate pressure p_2 satisfying the conservation of energy as shown in equation (5) and the conservation of mass $\dot{m}_N = \dot{m}_R$, which are shown below [20],

$$\dot{m}_N = c_2 \sin\alpha_2 \pi D_2 b_2 \rho_1 (\frac{p_2}{p_1})^{1/k}; \dot{m}_R = c_3 \sin\alpha_3 \pi D_3 b_3 \rho_2 \frac{T_2}{T_2^{'}} (\frac{p_3}{p_2})^{1/k} \tag{10}$$

Therefore, when the continuity of mass flow is satisfied, an average air flow within the stator/rotor stage is simulated and the performance of particular operation is estimated. Otherwise, if the two

mass flow rates are not equivalent, an iterative calculation has to be made to find the appropriate pressure ratios through the stator and rotor.

3.2. Heat exchanger

A two stream HEX is considered in this work, which can be elements of any design, i.e. brazed-plate, shell-and-tube or plate-and-plate frame. The HEX is modelled in one dimension which is parallel to the flow direction of the fluid. It is assumed that negligible conduction occurs in the direction of the flows compared to the convective heat transfer. A lumped overall heat transfer coefficient is used to estimate the heat transfer between the two streams. There is no heat source or sink inside the HEXs. Thermodynamic properties of the fluids across the discrete volumes, namely density and heat capacity of both compressed air and pressurised water in the LTA-CAES, are assumed to be constant at any time instant and the air properties are updated before the next time step based on the current pressure and temperature. In addition, with assumed sufficient volume and heat transfer area of the HEXs in the studied small-scale A-CAES system, velocities of the flows in the HEXs are relatively small compared to the speed of sound, resulting in the small Mach numbers of both flows. Thus, the simulation of HEXs assumes the incompressibility in both flows. Pressure drops of both fluids are not considered at the early stage. There is no phase-change of the fluids in the HEXs. In the LTA-CAES system, the water is pressurised to ensure its liquid state within the range of operating temperature.

Therefore, governing equations of the heat transfer within the HEXs are shown below,

$$\rho_h c_{p,h}\left(\frac{\partial T_h(x,t)}{\partial t} + v_h \frac{\partial T_h(x,t)}{\partial x}\right) = q_{w,h}$$
$$\rho_c c_{p,c}\left(\frac{\partial T_c(x,t)}{\partial t} + v_c \frac{\partial T_c(x,t)}{\partial x}\right) = q_{w,c} \quad (11)$$

where T is temperature of the fluid, c_p is heat capacity, ρ is density of the fluid. v is velocity of the fluid. Subscript h and c denote the hot fluid and cold fluid respectively. In this study, during the discharge period, compressed air (the cold fluid) is heated up through the HEX by the hot pressurised water flowing on the other side of the HEX. q_w is the source term representing heat flux across the HEX wall. The heat source term can be represented by

$$q_{W,h} = \frac{h_{HEX} A(T_c(x) - T_h(x))}{V_h}; q_{W,c} = \frac{h_{HEX} A(T_h(x) - T_c(x))}{V_c}; \quad (12)$$

where V is volume of the HEX, h_{HEX} is overall heat transfer coefficient.

As it is difficult to solve the partial differential equations (PDEs) analytically, this study uses finite difference method to solve the PDEs. Fig. 3(a) and Fig. 3(b) illustrate the discretisation of the flow channels of co-current HEX and counter-current HEX respectively. Each of the flow channels is discretised into a finite number of elements from the inlet to outlet.

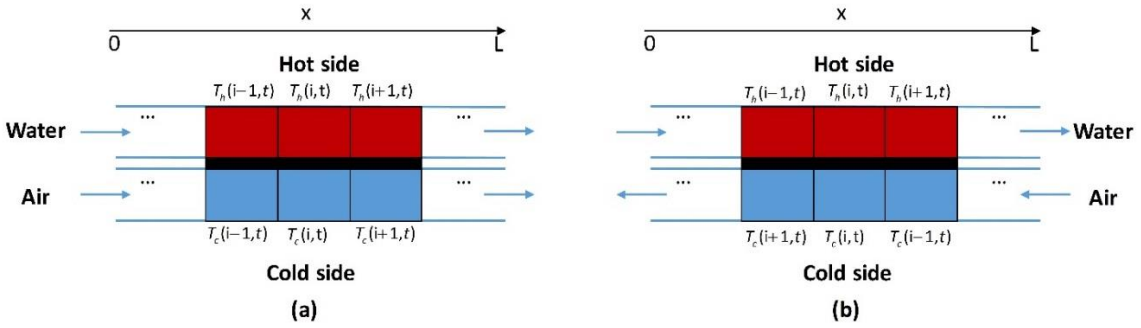

Figure 3 Illustrated diagram of HEX simulation. The co-current HEX is shown in (a) and the counter-current HEX is shown in (b).

Therefore, the finite difference method converts the PDEs to a system of algebraic equations, in which the convective term in the governing equation of both air and water is discretised using the first order upwind scheme. For simplicity, initial temperature distribution in both channels of the HEXs uses the constant value. With sufficient heat transfer area and volume, zero gradient boundary condition is set at the exits of both the flow channels. Consequently, boundary conditions and initial conditions of the co-current/counter-current HEXs are listed below,

$$T_h(x,0)=T_{W,0};T_c(x,0)=T_{A,0}$$

$$T_h|_{x=0}=T_{W,0};T_c|_{x=0}=T_{A,0};\frac{\partial T_h}{\partial x}|_{x=L}=0;\frac{\partial T_c}{\partial x}|_{x=L}=0 \quad \text{(co-current HEX)} \tag{13}$$

$$T_h|_{x=0}=T_{W,0};\frac{\partial T_c}{\partial x}|_{x=0}=0;\frac{\partial T_h}{\partial x}|_{x=L}=0;T_c|_{x=L}=T_{A,0} \quad \text{(counter-current HEX)}$$

where x is the coordinate of position and L is the length of the flow channel.

3.3. Electricity generator

The electricity generator can be either direct current (DC) or alternating current (AC). The investigated LTA-CAES system uses a DC electric generator to connect with the IFR turbine and generate electricity. In a separated excited DC generator, an external DC source supplies the field magnet winding. The equivalent circuit of a separated excited DC generator is illustrated in Fig. 4.

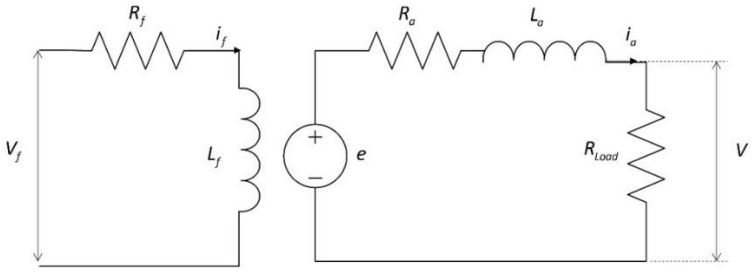

Figure 4 Illustrated resistance model of external excited DC generator.

Therefore, the DC generator's torque, τ_e, and back EMF, e, can be obtained, which are,

$$\tau_e = K_T i_a \tag{14}$$

$$e = K_E \omega_e \tag{15}$$

where K_T and K_E are torque constant and voltage constant respectively. ω_e is the rotational speed of the electric generator. In a separated excited DC machine, the voltage constant is proportional to the field current i_f, which is

$$K_E = L_{af} i_f \tag{16}$$

where L_{af} is the field-armature mutual inductance. According to Kirchhoff's circuit law, the circuit shown in Fig. 3 can be presented as

$$V_f = i_f R_f + L_f \frac{di_f}{dt} \tag{17}$$

$$e = i_a R_a + L_a \frac{di_a}{dt} + i_a R_{Load} \tag{18}$$

Substituting equation (15) into equation (18), the equation can be rewritten as

$$\frac{di_a}{dt} = \frac{K_E \omega_e - i_a (R_a + R_{Load})}{L_a} \tag{19}$$

where R_a is armature resistance, L_a is armature inductance, R_{load} is load resistance, i_a is armature current, R_f is field resistance.

Moreover, the summation of the moments of inertias determines the dynamics of turbine-generator rig. Inertias include the generator and the other components, because they are connected to the same shaft. On the basis of the angular momentum conservation, the transfer of the mechanical momentum can be described as,

$$\frac{d\omega_e}{dt} = \frac{\tau_t - \tau_e - \tau_{fri}}{J_t + J_e} \tag{20}$$

where τ_{fri} is mechanical losses due to friction, which is approximated by $\tau_{fri} = B_m \omega$, and B_m is the viscous friction coefficient. J_t and J_e are the momentum of inertia of turbine and electrical generator respectively. Substituting equation (14) into equation (20), the angular momentum balance can be further presented as

$$\frac{d\omega_e}{dt} = \frac{\tau_t - K_T i_a - B_m \omega_e}{J_t + J_e} \tag{21}$$

3.4. Water tank (heat/cold storage)

As sensible heat/cold storage in the LTA-CAES using the pressurised water, TES modelling is considered as water tank with an insulation layer. The model of heat/cold storage presents both hot and cold water storage in the A-CAES system. The following assumptions are taken into account for modelling the sensible TES: i) there is neither heat source nor sink in the water tank; ii) cylindrical shape water tanks are considered; iii) only the temperature and the height of the water in the tank are considered according to the incompressibility of water; iv) heat transfer between the water and air in the tank is not considered; v) pressure drops of flow are not considered. Therefore, model of the water tank is presented as,

$$\frac{dT_{wt}}{dt} = \frac{(m_{in,w}h_{in,w} - m_{out,w}h_{out,w})}{c_{P,w}\rho_w A_{wt}H_{wt}} - \frac{h_{wt}\,\mathrm{A}\,(T_{wt} - T_s)}{c_{P,w}\rho_w A_{wt}H_{wt}}$$
$$\frac{dH_{wt}}{dt} = \frac{m_{in,w} - m_{out,w}}{\rho_w A_{wt}} \quad (22)$$

where $m_{in,w}$ and $m_{out,W}$ are the mass flow rate of the water at inlet and outlet of the water tank. $h_{in,w}$ and $h_{out,w}$ are enthalpy of water at the inlet and the outlet, which are $h_{in,w} = c_{p,w}(T_{out,w} - T_{wt})$ and $h_{out,w} = c_{p,w}(T_{in,w} - T_{wt})$. H_{wt} is the height of the water level in the tank. A_{wt} and A_{ws} are the bottom area and surface area of the water tank. h_{wt} is the overall heat transfer coefficient between the TES tank and ambience.

To consider the overall heat transfer coefficient between the internal water and ambience, Fig. 5 illustrates the heat transfer model using thermal resistances. Thus, the thermal resistance model utilises an overall heat transfer coefficient to estimate the heat transfer through the insulation material and the tank wall to ambience in radial direction. From the fluid inside the tank to ambience, there are three thermal resistance layers. For simplicity, it is assumed that the temperature of the tank wall is equivalent to that of the ambient air, namely $T_w = T_\infty$.

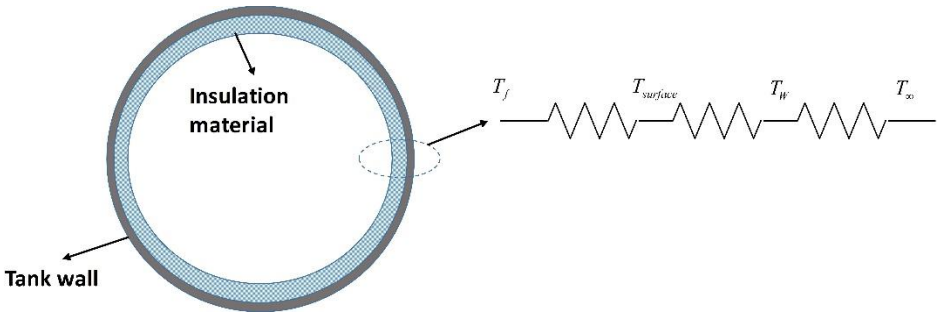

Figure 5 Illustrated resistance model of the overall heat transfer coefficient of heat dissipation to the ambience.

Then, energy balance can be obtained based on the heat flux in the radial direction,

$$\frac{2\pi H k_{insulation}}{\ln(D_{out}/D_{in})}(T_f - T_{surface}) = h_{wall}\pi D_{out}H(T_{surface} - T_\infty) \quad (23)$$

where $k_{insulation}$ is heat conductivity of the insulation material, and h_{wall} is natural heat transfer coefficient between the tank wall and ambience. h_{wall} can be obtained using [21]

$$Nu(x) = [\frac{7Gr(x)\,\mathrm{Pr}^2}{100+105\,\mathrm{Pr}}]^{1/4} + \frac{4(272+315\,\mathrm{Pr})}{35(64+63\,\mathrm{Pr})}\frac{x}{D_0} = \frac{h_{wall}}{k_f}; Gr(x) = \frac{g(T_{surface} - T_w)x^3}{\nu^2(T_{surface} + T_w)} \quad (24)$$

where x denotes the axial position of the water tank. Therefore, the overall heat transfer is [21]

$$\frac{1}{h_{wt}} = \frac{D_r \ln(D_{out}/D_{in})}{2k_{insulation}} + \frac{1}{h_{wall}}\frac{D_r}{D_{out}} \quad (25)$$

where D_r is the reference diameter paired with the overall heat transfer coefficient.

3.5. Air storage tank

An air tank is used as the compressed air storage. It is assumed that neither source nor sink is in the tank. Besides air temperature variation, density and pressure of the air in the tank change during the A-CAES operations. Therefore, based on the mass and energy conservations, the governing equations describing compressed air in the air tank are [22],

$$\begin{aligned} \frac{d\rho_{at}}{dt} &= \frac{m_{in,a} - m_{out,a}}{V_{at}} \\ \frac{d(mU)}{dt} &= (m_{in,a}h_{in,a} - m_{out,a}h_{out,a}) - h_{at}\,A_{as}(T_{at} - T_s) \end{aligned} \tag{26}$$

where subscript at denotes air tank. $m_{in,a}$ and $m_{out,a}$ are the mass flow rate of the air at inlet and outlet of the air tank. $h_{in,a}$ and $h_{out,a}$ are enthalpy of air at the inlet and the outlet, which are $h_{in,a} = c_p(T_{out,a} - T_{at})$ and $h_{out,a} = c_p(T_{in,a} - T_{at})$. A_{as} is the surface area of the air tank. h_{at} is the overall heat transfer coefficient between the air tank and ambience.

Using the ideal gas theory, internal energy of the compressed air in the storage can be presented as,

$$U = h - P/\rho; dh = c_p dT \tag{27}$$

Therefore, substituting equation (27) into energy equation shown in (26) leads to [22]

$$\rho_{at} c_P \frac{dT}{dt} + \frac{m_{in,a}}{V_{at}} c_p (T_{at} - T_{in}) - \frac{dP_{at}}{dt} + \frac{h_{at}A_{at}}{V_{at}}(T_{at} - T_s) = 0 \tag{28}$$

Substituting temperature derivative expressed by equation (28) to the state equation of ideal air, variation of air pressure in the storage tank can be obtained

$$\frac{dP}{dt} = \frac{1}{V_{at}}(\kappa R T_{in,a} \dot{m}_{in,a} - \kappa R T \dot{m}_{out,a} + (\kappa - 1) h_{at} A_{at}(T_{at} - T_s)) \tag{29}$$

Using the proposed lumped volumetric heat transfer coefficient in [22], an experimental correlation is fitted,

$$h_{eff} = \frac{h_{at}A_{at}}{V_{at}} = a + b\left|m_{in,a} - m_{out,a}\right|^{0.8} \tag{30}$$

where a and b represent the heat transfer coefficient caused by natural convection and forced convection in the storage.

3.6. Throttle valve

Air flow through the throttle valve is assumed to be isenthalpy processes, which satisfies

$$h_u = h_d \tag{31}$$

where the subscript u and d present the upstream and downstream of the valve.

4. Dynamic modelling of the low temperature Adiabatic Compressed Air Energy Storage system from the component level mathematical models

The whole system dynamic modelling is conducted by assembling all the models of the associated components. By tracking the working fluids' thermodynamic variables, namely the compressed air and the pressurised water, through inlets and outlets of the components, and interactions in between, the

component models are interconnected together to simulate the transitions and performance of the whole system. The process irreversibility is the accumulation of the exergy losses in every components that results in the whole system losses. The exergy decreases of both the fluids considered in the LTA-CAES system discharging include air pressure drop in the air tank, water temperature reduction from the hot water tank to the normal water tank, heat dissipations to ambience of the both air and water tanks, throttling losses, flow losses (frictional losses and incidence losses) in the turbines, and exhaust air loss. All of these exergy variations of air and water are mathematically described in the system model presented in Section 3. Among them, the air pressure drop and the water temperature decrease in the water tank can be recovered by combining the charging to fulfil the full energy storage cycle. This study does not consider thermal inertias/resistances caused by the casting of components, pressure drops of flow in pipes/channels, and thermal losses of generators.

Fig. 6 shows the dynamic modelling framework of the LTA-CAES discharge system structure. At the beginning of the simulation, parameter initialisation is needed for all the component-level models, such as design parameters of the air tank and the water tanks, geometric parameters of the radial turbines, and parameters of the generator. At each time step, variables including pressure, temperature and mass flow rate are simulated when the compressed air and the pressurised water flow through different components in all the three stages. The speed-torque characteristics of the shaft are calculated through the mechanical power transmission between the turbines and the generator. The derivatives of these variables with respect to time are calculated based on the variables at the current time step. These variable variations update the variables for the next time step. This study builds up the component mathematical models using MATLAB programming/scripting and assembles the whole system in Simulink environment to study its dynamic behaviour. Therefore, the built-up ordinary differential equations are solved by ODE solvers in MATLAB/SIMULINK.

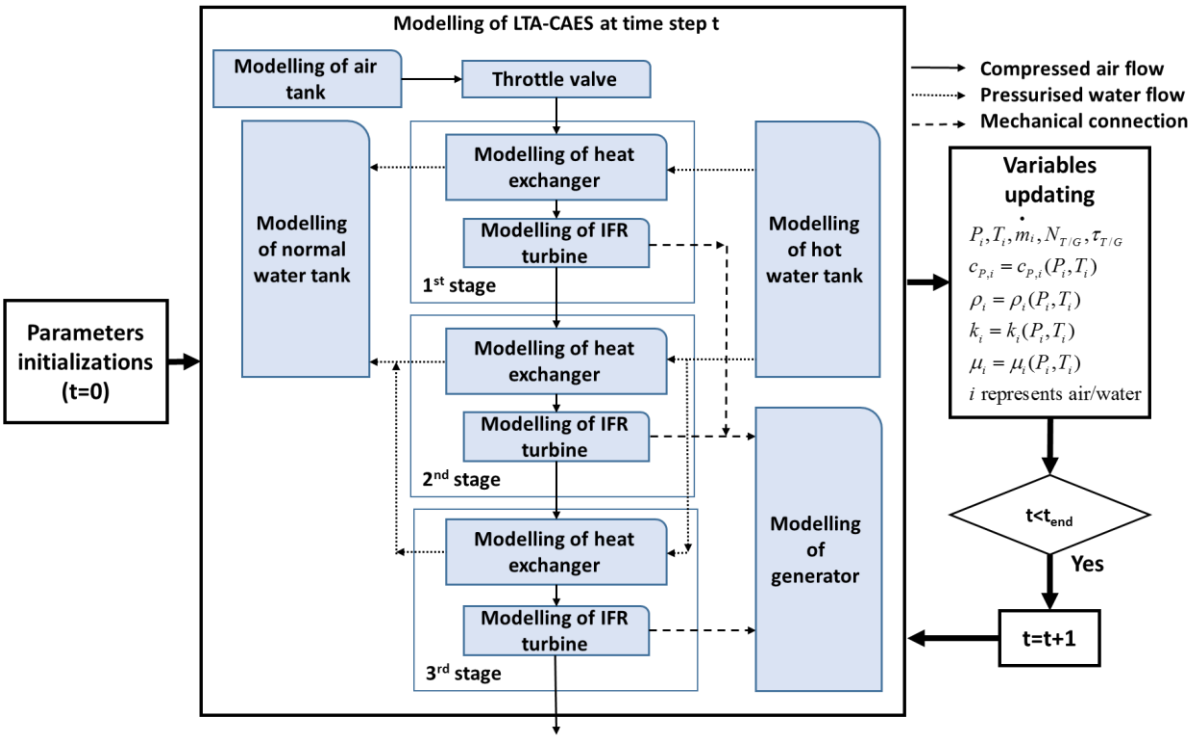

Figure 6 Schematic flowchart of dynamic modelling framework.

As stated in [23], ideal gas theory has limitations in applications of A-CAES and real gas properties of air need to be considered. Deviations of air properties between the ideal and real gas theories

increase when air has high pressure, and decrease when air has high temperature [24, 25]. Consequently, in a LTA-CAES system, the ideal gas theory may have large deviations due to the relatively high pressure and low temperature in the operations. Therefore, the real gas effect is considered in the modelling using *CoolProp*, which is an open-source thermophysical property library which implements a series of thermophysical property correlations [26]. Thermodynamic properties, such as heat capacity, density, viscosity and heat conductivity, of both the compressed air and the pressurised water are updated using current pressure and temperature at each time step.

5. Results and discussion

With the model developed above, this Section presents the simulations of the dynamic LTA-CAES system behaviours.

5.1. Validation of mathematical models of the components models and the system dynamic model

Before carrying out the analysis of the LTA-CAES by simulations, validations of these mathematical models are first presented. In all the components, performance prediction of the turbine is the most complicated due to the complex flow and design of the machine. Thus, validation of the one dimension model is carried out by comparing the performance curves between the simulation and experimental data. The test data of a high pressure radial turbine is used in the validation and the parameters of the turbine are listed in Table 1. Fig. 7 shows the comparisons of the experimental and simulation results. The detailed experimental parameters and the experimental performance curves can be found in [27]. As shown in Fig. 7, the performance curve shows the acceptable agreement between the experimental data and the simulation data. So the component-level mathematical model of the IFR turbine is capable of predicting the performance of the turbine over a wide range of operation status with different pressure ratios and rotational speeds.

Table 1 Parameters used in the validation of the turbine modelling. The parameters are read from [27].

Design parameter	Value	Geometric parameter	Value
Pressure ratio	5.73	Rotor inlet diameter, m	0.058
Inlet pressure, MPa	0.58	Rotor outlet mean diameter, m	0.026
Rotational speed, rpm	106,588	Rotor inlet width, m	0.006
Inlet temperature, °C	784	Rotor outlet width, m	0.021
Efficiency	87%	Rotor outlet angle, degree	57.4
Shaft power, kW	38	Nozzle outlet angle, degree	77.6

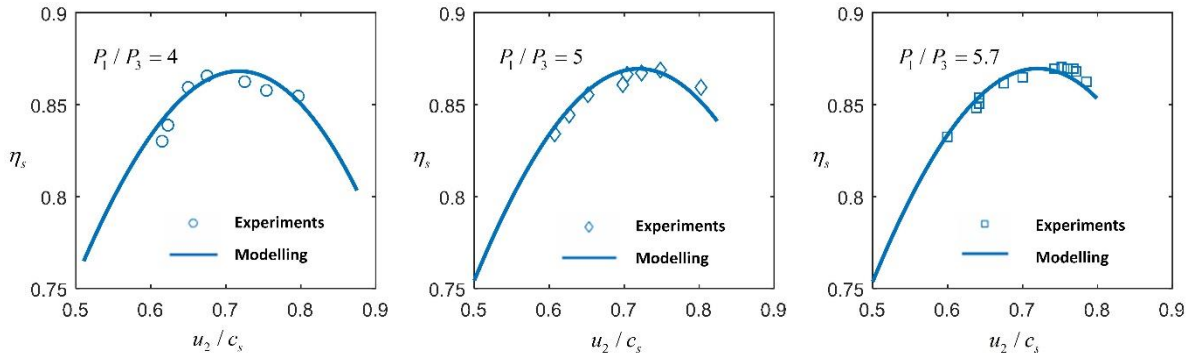

Figure 7 validation of the mathematical model of IFR turbine.

Additionally, for the validation of air storage tank modelling, the published data and cavern parameters from Huntorf plant are used in validation [22, 28]. Compared to the air storage tank in the LTA-CAES system in this work, Huntorf CAES plant also uses the isochoric storage, namely constant-volume air storage. Thus, both the air storage can be described by the same mathematical models with different specifications of geometry and materials. The parameters of the cavern for air storage in Huntorf CAES plant is listed in Table 2. A variable air mass flow rates during the discharge from the experimental data [22, 28] is used as input, which is shown in Fig. 8(a). The pressure and temperature variations during the discharge process are presented in Fig. 8(b) and 8(c), respectively. It indicates that the modelling results agree with experimental data reasonably well.

Table 2 Parameters of the cavern for air storage in Huntorf CAES plant. The parameters are from [22]

Parameter	Value
Air storage volume, m^3	300,000
Air storage pressure range, MPa	4.6-6.6
Maximum cavern, MPa	7.2
Cavern wall temperature, °C	~50
Maximum discharge rate, MPa/h	0.1

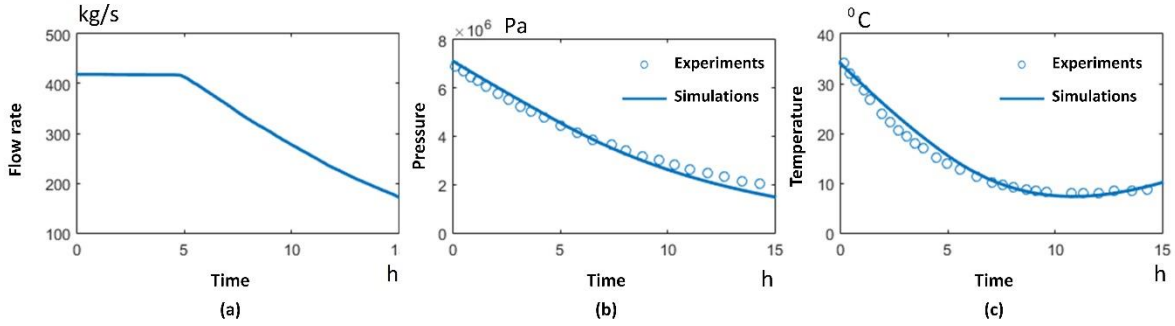

Figure 8 validation of mathematical model of air storage tank.

At the system-level, the dynamic modelling is validated using the experimental data of the "TICC-500" pilot plant [3]. Parameters of the system are listed in Table 3. In order to carry out component-level modelling of the radial turbine, basic geometric parameters are needed for the simulation. Therefore, based on the design parameters as shown in Table 3, this work estimates the geometric parameters of the IFR turbines in three stages. The estimated parameters are shown in Table 4. For operating the turbines in a range close to the design points, the simulation regulates the inlet pressure to the design inlet pressure in every turbine-stage, if the inlet pressure is higher than the designed value. As shown in Table 3, the highest water temperature of hot water tank is 108.2 °C and the hydraulic pressure of water is 4 bar. The phase-changing temperature of water from the liquid state to the gas state is approximately 143 °C, when the pressure of water is 4 bar. Thus, in the studied operations of the "TICC-500" pilot plant, there is no two-phase flow of water in the hot water tank, the HEXs, the normal water tank and pipes.

Through the comparisons, the performance of all the turbines are close to the performance of those of designed operations. Because the optimum designs of these turbines are beyond the scope of this study, these estimated geometric parameters are used to simulate the performance curve of turbines at the system-level. In addition, a set of the gearbox and DC generators are also paired with

turbines. Energy loss is not considered in the mechanical transmission by the gearbox. Other parameters used in the simulations are listed in Table 5. As the linear relationship between power and torque of DC generators, at the early stage, a set of three 225HP (about 168 kW) DC generators are bounded to present the 500 kW generator.

Table 3 Parameters of "TICC-500" pilot A-CAES plant from [3].

Parameter	Value
Air storage volume, m^3	100
Air storage pressure range, MPa	2.5-9.5
Pressure of water, MPa	0.4
Water tank volume, m^3	12
Initial temperature of hot water tank, °C	108.2
Rated air mass flow rate, kg/h	8600
Rated speed, rpm	30,000
First stage turbine	
Inlet pressure, MPa	2.50
Rated outlet pressure, MPa	1.13
Inlet temperature, °C	100
Rated outlet temperature, °C	35
Rated adiabatic efficiency	82.6%
Rated shaft power, kW	150.5
Second stage turbine	
Inlet pressure, MPa	1.12
Rated outlet pressure, MPa	0.4
Inlet temperature, °C	100
Rated outlet temperature, °C	25
Rated adiabatic efficiency	81.0%
Rated shaft power, kW	185.5
Third stage turbine	
Inlet pressure, MPa	0.39
Rated outlet pressure, MPa	0.1
Inlet temperature, °C	100
Rated outlet temperature, °C	0.5
Rated adiabatic efficiency	81.6%
Rated shaft power, kW	236.3

Table 4 Estimated geometric parameters of the three stage turbines and simulated performance.

Operational parameter	Value	Geometric parameter	Value
First stage turbine			
Inlet pressure, MPa	2.50	Rotor inlet diameter, m	0.1728
Outlet pressure, MPa	1.13	Rotor outlet mean diameter, m	0.0773
Inlet temperature, °C	100	Rotor inlet width, m	0.0044
Outlet temperature, °C	34.36	Rotor outlet width, m	0.0148
Adiabatic efficiency	82.34%	Nozzle outlet angle, degree	77
Shaft power, kW	149.4	Rotor outlet angle, degree	56.1
Second stage turbine			
Inlet pressure, MPa	1.12	Rotor inlet diameter, m	0.2226

Outlet pressure, MPa	0.4	Rotor outlet mean diameter, m	0.1050
Inlet temperature, °C	100	Rotor inlet width, m	0.0074
Outlet temperature, °C	18.23	Rotor outlet width, m	0.0253
Adiabatic efficiency	80.3%	Nozzle outlet angle, degree	77
Shaft power, kW	181.4	Rotor outlet angle, degree	56.1
Third stage turbine			
Inlet pressure, MPa	0.39	Rotor inlet diameter, m	0.2515
Outlet pressure, MPa	0.1	Rotor outlet mean diameter, m	0.1144
Inlet temperature, °C	100	Rotor inlet width, m	0.0192
Outlet temperature, °C	0.03	Rotor outlet width, m	0.0642
Adiabatic efficiency	78.72%	Nozzle outlet angle, degree	77
Shaft power, kW	225.2	Rotor outlet angle, degree	56.1

Table 5 Parameters used in the simulations.

Parameter	Value
Armature resistance, Ω [29]	0.07571
Armature inductance, H [29]	0.001986
Field resistance, Ω [29]	33.46
Field inductance, H [29]	3.499
Field armature mutual inductance, H [29]	0.2874
Inertia, $\mathrm{kg \cdot m^2}$ [29]	0.9177
Viscous friction torque, $\mathrm{N \cdot m \cdot s}$ [29]	0.02289
Transmission ratio of gearbox	18
Transmission efficiency of gearbox	100%
HEX overall heat transfer coefficient, $\mathrm{W \cdot m^{-2} \cdot K^{-1}}$	100
Diameter of TES tank, m	2
Height of TES tank, m	3
Averaged mass flow rate, kg/h [3]	7760

With the parameters listed in Tables 3, 4 and 5, dynamic modelling of the discharge process of the LTA-CAES system as shown in Fig. 1 is developed. Several results of the system during the discharge period are plotted in Fig. 9, including both the experimental data from [3] and the simulation results of temperature and pressure in storage tank in (a) and (b), rotational speed of the turbine in (c) and the inlet temperature of turbines in the three stages in (d), (e) and (f), respectively. As shown in these figures, although the experimental data may fluctuates during the discharge period, the simulated results closely track the dynamic responses of components in the system. In Fig. (d), (e) and (f), the simulation results agree with the experimental data during the quasi-steady-state operation (after about 5 mins) with a slight deviation between the experimental data and simulation at the beginning. This deviation is mainly caused by the inaccuracy of the initial condition's setting in simulating the HEXs, but the different initial temperature profiles' setting in the HEXs also gives an opportunity to analyse the thermal initial condition of the HEXs in the system dynamic modelling. With the insulation, heat losses of the water is negligible in the hot water tank to ambience during the 50 min discharging period. The water temperature in the hot water tank becomes 108.1 $^{\circ}\mathrm{C}$. Because of the normal water tank is positioned on the downstream of the HEXs and the turbines, the water temperature in the tank does not affect the performance of the turbines in the current discharging period. Without the parameters and initial condition of the normal water tank from [28], the temperature is not analysed in this work.

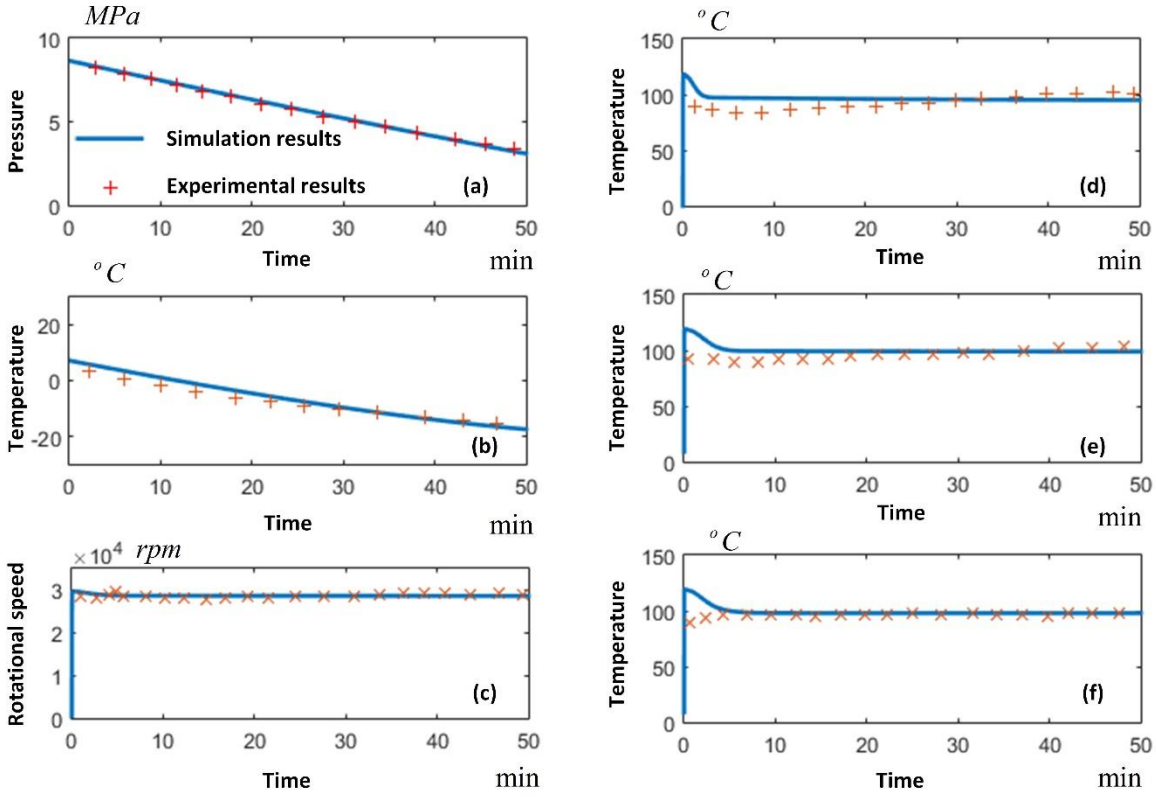

Figure 9 Validation of system level dynamic modelling framework.

5.2. Start-up of the low temperature Adiabatic Compressed Air Energy Storage discharge

In the simulation, there is a slight decrease of the rotational speed of the turbine after the rapid increase at the beginning during the start-up. In fact, the start-up can be divided into two periods. In the first period, speed of the shaft increases rapidly due to the mechanical energy conversion between the compressed air and the rotating shaft. It is governed by Equation (21) in which the changing rate of the speed is influenced by the mechanical inertias connected to the shaft. Furthermore, the speed gradually reduces to a certain level, which is a result of the delayed effect due to the thermal inertia of heat transfer in the HEXs. As shown in Fig. 9(d), 9(e) and 9(f), because of the slowly established steady temperature of the compressed air at the outlet of the HEXs, torques produced by the turbines are affected. Consequently, these responses of heat transfer slow down building up the whole system's steady-state operation.

To overcome this delayed thermal effect as simulated, in practice, at the start-up, the turbine is usually operated first without connection with a generator. In order to gradually increase the temperature of flowing air or casting, the turbine may be held in a lower speed initially and gradually increasing to the rated value. When it rotates at the rated speed, if temperature distribution inside the turbine is acceptable and inlet condition of air becomes steady, the external torque connects with the turbine. This is how the steam turbine in a power plant operates in a "cold-start".

Furthermore, based on the mathematical model of the HEXs and dynamic modelling of the LTA-CAES system, other possible configurations, such as the counter-current HEX, can be considered using the basic models as presented by equation (11), (12) and (13). As shown in Fig. 1, the "TICC-500" pilot plant utilised the co-current flow scheme of HEXs. It is well-known that the counter-current HEX configuration has higher effectiveness than the co-current configuration. The outlet temperature of the cold stream is possibly higher than that of the hot stream at the inlet of a counter-current HEX. In contrast, the temperature of the cold stream cannot exceed the hot stream through the inlet to outlet

in a co-current configuration. Therefore, both the co-current and counter-current HEXs are simulated and the influenced dynamic system performances are compared.

In the simulations of the counter-current HEX using equation (11)-(13), since flow directions of two fluids are different, pairing the control volumes in the two flow channels to calculate the source term of heat flux across the wall is essential. The results of the LTA-CAES discharge are shown in Fig. 10 and 11 in which the rotational speed is plotted in Fig. 10, and inlet temperature of the air flowing to the turbine in the three stages are plotted in Figure. 11. To compare the two flow schemes of the HEXs, all the simulations use the same parameters listed in Table 3, 4 and 5.

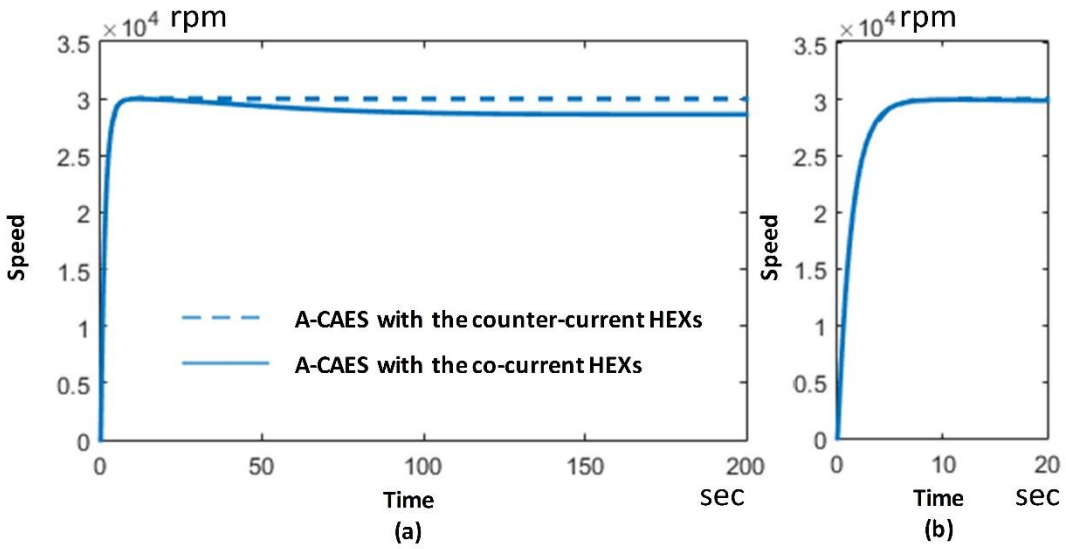

Figure 10 The rotation speed of the shaft of A-CAES plants with co-current and counter-current HEXs in Fig. 10(a). The rising speed of the shaft at the beginning is particularly plotted in Fig. 10(b).

According to the results in Fig 10(a), it clearly indicates the faster steady-state response and higher effectiveness of the counter-current HEXs than the co-current HEXs. Although both the two A-CAES systems have almost identical rapid speed increase at the first several seconds as shown in Fig. 10(b), the system using the counter-current HEXs reaches a higher steady-state speed. There is a negligible decrease of the speed caused by the reduced thermal effect in the system using the counter-current HEXs in comparison to that using the co-current HEXs.

In fact, the fast response of the counter-current HEXs is a result of the enhanced mean net temperature difference and heat flux across the wall. With the same hot water stream (both the same temperature and flow rate), the improved heat transfer leads to higher temperature of the compressed air leaving the counter-current HEXs than that in the co-current HEXs, which is shown in Fig. 11. Because the initial very large rate of the air temperature increase in both systems is significantly caused by the initial condition for air temperature in the modelling, the focus of the simulation is on the physical dynamics of the heat transfer regardless of the initial temperature profiles, which is the varying temperature after the rapid increasing. As shown in Fig. 11(a), (c) and (e), compared to the co-current HEXs, there is no significant temperature decrease in the counter-current HEXs after the rapidly rising temperature at the beginning. Actually, air temperature in the counter-current HEXs also decreases but in a much modest way, which are shown in Fig. 11(b), (d) and (f). These achieved high steady-state air temperature in all the three stages improves the system response. Also, more input exergy of the compressed air flows to the turbine in every stage. These extra exergies produce more torques to drive the generator to a fast speed with the given electric load.

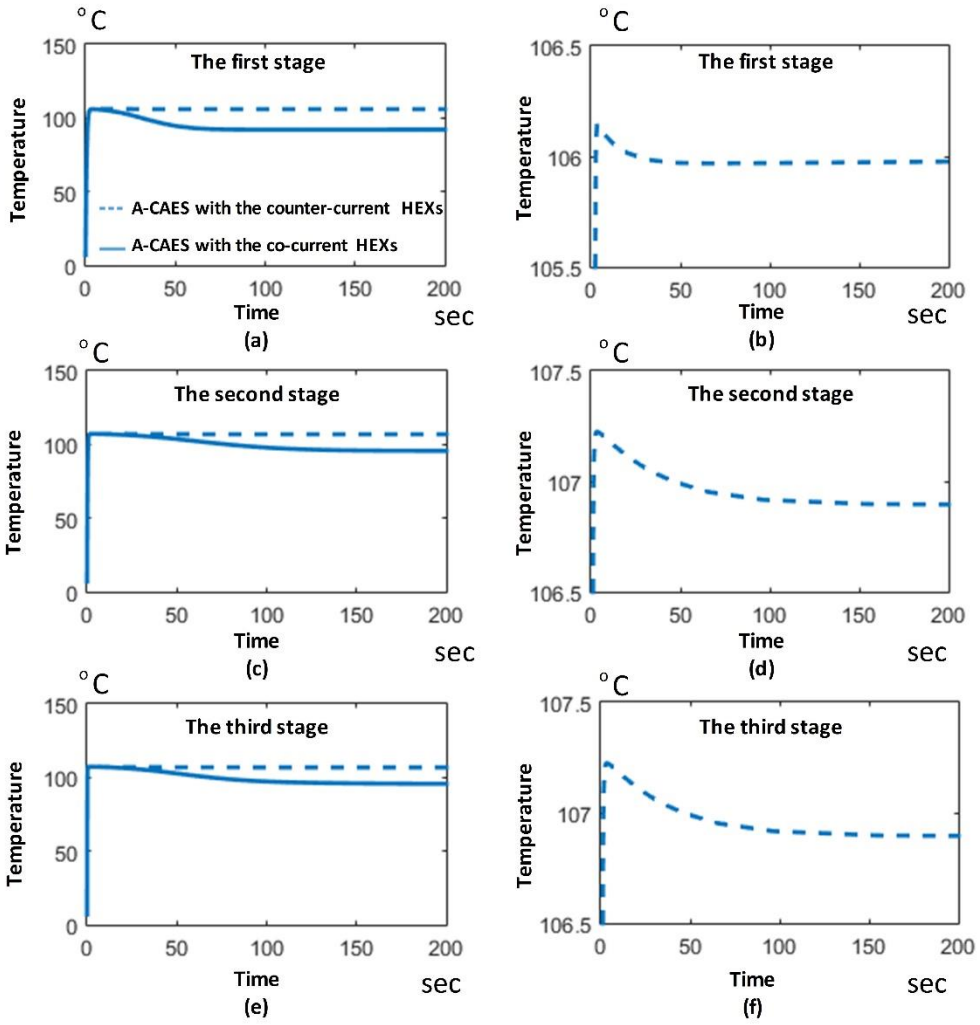

Figure 11 Temperature of compressed air at the inlet of the turbine in each stage.

5.3. Effect of part-load operation of turbine in the low temperature Adiabatic Compressed Air Energy Storage discharge

As an energy storage technology, flexible operation subject to a changing load or demand is a common application. Thus, this section presents a study of the operational transition due to a variable electric load. To follow the variable load, the A-CAES system is operated and controlled over a range of operations. In the discharge period, because of the difficulty to change the rotational speed of turbine-generator set, the rotational speed is maintained constant after the start-up [30]. To match the changed electric load without change of shaft speed, mass flow rate of the air flowing to the turbine is altered and controlled. Mass flow rate is controlled through changing the valve or inlet guide vane of the turbine at the first stage. In this study, the changing mass flow rate is achieved by a controller for tracking a reference rotational speed. The mass flow rate is assumed to be achieved by changing the displacement of valves in the first stage. Accordingly, performance of both the components and system will be changed due to the varied mass flow rate. This section aims to study how these variations occur dynamically and track the changed system performance due to the operation transitions.

Fig. 12 illustrates the diagram of the LTA-CAES with a PD controller. It needs to be noted that other control strategies are potentially feasible subject to applications. The reference speed uses the steady-state rotational speed with the electric load during the start-up. A signal pulse of the PD controller is

selected as 1 second in the simulation, which can be changed according to the particular applications and experimental facilities. The tuned coefficients of the PD controller are proportional coefficient 0.5×10^{-4} $\mathrm{kg/(s\cdot rpm)}$ and derivative coefficient 0.1×10^{-5} $\mathrm{kg/rpm}$. The varied electric load represents the variable power demand in practice. In power network, during the peak time, power load increases and equivalent electrical resistance load decreases. In contrast, power load decreases and equivalent electrical resistance load increases during the off-peak time. The followed profile of the variable equivalent resistance load to the electric generator is shown in Fig. 13, which starts at 1.45 Ω for the first 200 seconds, then gradually increases to 1.85 Ω, and finally decreases back to 1.45 Ω by a step size of 0.1 Ω in sample period of 50 s. It needs to be noted that the selected variable load fitted to operation between 100% and approximated 80% partial load. During the start-up, the controller is deactivated and let the system change to the steady-state operation. Then, the controller is activated at the time of 150 second. The operation exemplifies the capability of the dynamic modelling framework to study the transient behaviour of the LTA-CAES discharge. The modelling library and framework can also simulate other possible variable loads.

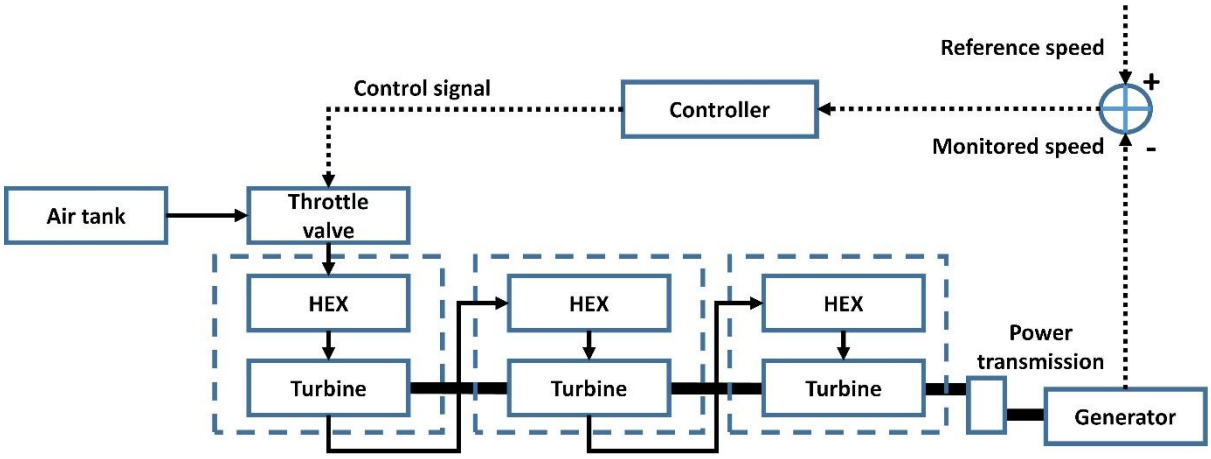

Figure 12 Illustrated diagram of PD controller in rotational speed tracking.

Fig. (14)-(17) show the results of the dynamic responses of the LTA-CAES by following the variable load profile, in which the rotational speed is shown in Fig. (14), the mass flow rate is in Fig. (15), total output power of all three stages is presented in Fig. (16), and the isentropic efficiency of the first-stage turbine is illustrated in Fig. (17). As show in Fig. 14, when the electrical load varies, the rotational speed tends to establish a new balance between power generation and consumption. The sudden decrease of electrical power load causes a decrease of current and external torque connected with the turbines. The controller detects this sudden variation, automatically changes the mass flow rate to meet the variable load and tracks the reference rotational speed. As shown in Fig. 14, although the rotational speed slightly fluctuates around the reference speed, the operation transitions only take several seconds back to the reference value based on the selected control signal frequency in the simulations. The performance can be further improved by optimally selecting the controller strategy, which can be investigated further using the proposed dynamic modelling method.

In addition, with the increase of electrical load to the generator, mass flow rate reduces in order to meet the decreased external torque. The power generated from the turbines is also decreased to accommodate to the decreased power consumption. As shown in Fig. 15 and 16, the mass flow rate and power output slightly fluctuate at the beginning of each load changing period and gradually change to the new steady-state values.

Because the geometric parameters of turbines are optimised for the design operations, the isentropic efficiency is lower when the machines are operated away from the design operation status. In these off-design operations, as the mass flow rate of the air decreases, the relative flow angle at the inlet of the rotor would be less than the design angle. Energy losses due to the progressive flow separation that is initially formed at the front of the suction surface are detrimental to the machine's efficiency. As plotted in Fig 17, using the first-stage turbine as an example, the reduced isentropic efficiencies are found in its partial load operations with low mass flow rates when the connecting electrical load is changing.

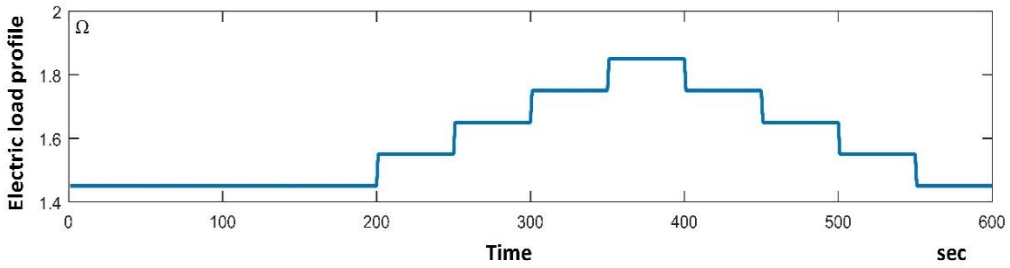

Figure 13 Studied variable electrical load profile.

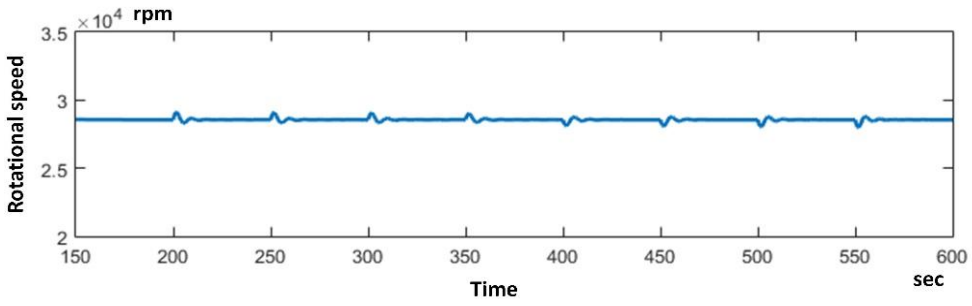

Figure 14 Rotational speed during the transient operations.

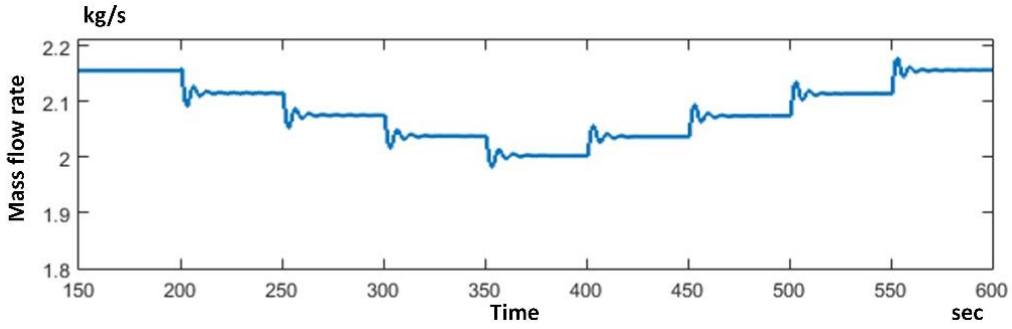

Figure 15 Mass flow rate during the transient operations.

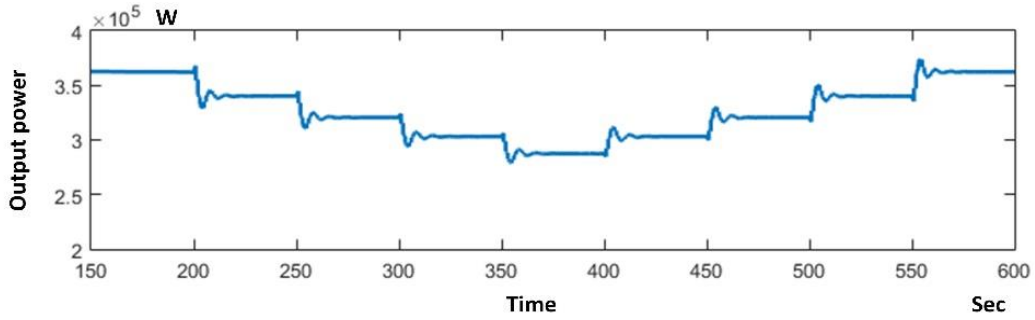

625

626 **Figure 16** Output power generated of the three stages turbines during the transient operations.

627

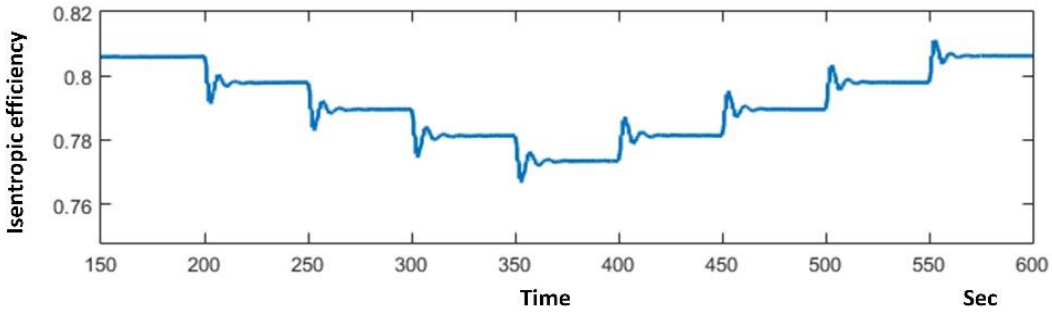

628

629 **Figure 17** Isentropic efficiency of the first stage turbine during the transient operations.

630

631 ## 6. Conclusion

632 With the proposed "quasi dynamic iterative searching" method, a simulation platform of the LTA-
633 CAES with radial turbines is built for analysing the system responses arisen by operation status change,
634 heat transfer, mechanical transmission and energy conversions. In order to verify the proposed
635 simulation platform and the associated components' models, simulation results are validated using
636 experimental data from the published works. Then, a particular case study of the LTA-CAES system
637 discharging LTA-CAES is developed to analyse the system transience during start-up and operational
638 transitions. Based on the results, several conclusions can be drawn: 1) The developed simulation
639 platform of the LTA-CAES with radial turbines using the "quasi-dynamic iterative searching" shows
640 satisfactory agreement with the experimental data. 2) Based on the proposed simulation platform,
641 multiple time scales of the system responses are analysed in the LTA-CAES system discharging during
642 the start-up and operation transitions. The LTA-CAES system shows fast mechanical responses of the
643 shaft and slow thermal responses due to heat transfer in the HEXs during the start-up of discharging.
644 3) The LTA-CAES system with the counter-current HEXs has higher rotating speed in the steady-state
645 because of the enhanced heat transfer between the two fluids, compared to the LTA-CAES system
646 with the co-current HEXs. 4) The work demonstrates the compatibility of dynamic modelling
647 framework to combine with the controller for tracking a constant rotational speed subject to a variable
648 electric load. 5) In the operational transitions, when the electrical load increases, the air mass flow
649 rate decreases, matching the power generation to the reduced power load, and maintaining the
650 reference rotating speed. However, the incidence loss arisen by the decreased flow rate from the
651 design operation results in the turbine efficiency drop.

652

Acknowledgments:

The authors would like to thank the funding support from Engineering and Physical Science Research Council (EPSRC), UK (EP/L014211/1 and EP/L019469/1). The authors also want to thank the support from China 973 Research Programme (2015CB251301) to enable the discussion with Chinese partners.

Reference:

[1] Wolf D, Budt M. LTA-CAES – A low-temperature approach to Adiabatic Compressed Air Energy Storage. Applied Energy. 2014;125:158-64.
[2] Luo X, Wang J, Krupke C, Wang Y, Sheng Y, Li J, et al. Modelling study, efficiency analysis and optimisation of large-scale Adiabatic Compressed Air Energy Storage systems with low-temperature thermal storage. Applied Energy. 2016;162:589-600.
[3] Wang S, Zhang X, Yang L, Zhou Y, Wang J. Experimental study of compressed air energy storage system with thermal energy storage. Energy. 2016;103:182-91.
[4] Sun H, Luo X, Wang J. Feasibility study of a hybrid wind turbine system – Integration with compressed air energy storage. Applied Energy. 2015;137:617-28.
[5] Krupke C, Wang J, Clarke J, Luo X. Modeling and Experimental Study of a Wind Turbine System in Hybrid Connection With Compressed Air Energy Storage. IEEE Transactions on Energy Conversion. 2017;32:137-45.
[6] Liu J-L, Wang J-H. A comparative research of two adiabatic compressed air energy storage systems. Energy Conversion and Management. 2016;108:566-78.
[7] Yao E, Wang H, Wang L, Xi G, Maréchal F. Thermo-economic optimization of a combined cooling, heating and power system based on small-scale compressed air energy storage. Energy Conversion and Management. 2016;118:377-86.
[8] Guo Z, Deng G, Fan Y, Chen G. Performance optimization of adiabatic compressed air energy storage with ejector technology. Applied Thermal Engineering. 2016;94:193-7.
[9] Paltrinieri A. A mean-line model to predict the design performance of radial inflow turbines in organic rankine cycles. 2014.
[10] Bao J, Zhao L. A review of working fluid and expander selections for organic Rankine cycle. Renewable and Sustainable Energy Reviews. 2013;24:325-42.
[11] Arabkoohsar A, Machado L, Koury RNN. Operation analysis of a photovoltaic plant integrated with a compressed air energy storage system and a city gate station. Energy. 2016;98:78-91.
[12] Wolf D. Methods for Design and Application of Adiabatic Compressed Air Energy: Storage Based on Dynamic Modeling: Laufen; 2011.
[13] Sciacovelli A, Li Y, Chen H, Wu Y, Wang J, Garvey S, et al. Dynamic simulation of Adiabatic Compressed Air Energy Storage (A-CAES) plant with integrated thermal storage – Link between components performance and plant performance. Applied Energy. 2017;185, Part 1:16-28.
[14] Li Y, Sciacovelli A, Peng X, Radcliffe J, Ding Y. Integrating compressed air energy storage with a diesel engine for electricity generation in isolated areas. Applied Energy. 2016;171:26-36.
[15] Zhao P, Gao L, Wang J, Dai Y. Energy efficiency analysis and off-design analysis of two different discharge modes for compressed air energy storage system using axial turbines. Renewable Energy. 2016;85:1164-77.
[16] Briola S, Di Marco P, Gabbrielli R, Riccardi J. A novel mathematical model for the performance assessment of diabatic compressed air energy storage systems including the turbomachinery characteristic curves. Applied Energy. 2016;178:758-72.
[17] van Putten H, Colonna P. Dynamic modeling of steam power cycles: Part II – Simulation of a small simple Rankine cycle system. Applied Thermal Engineering. 2007;27:2566-82.
[18] Dixon S. Fluid mechanics, thermodynamics of turbomachinery. in si/metric units. 1978.

[19] Dixon SL, Hall C. Fluid mechanics and thermodynamics of turbomachinery: Butterworth-Heinemann; 2013.
[20] Wallace F. Theoretical assessment of the performance characteristics of inward radial flow turbines. Proceedings of the Institution of Mechanical Engineers. 1958;172:931-52.
[21] Peng H, Dong H, Ling X. Thermal investigation of PCM-based high temperature thermal energy storage in packed bed. Energy Conversion and Management. 2014;81:420-7.
[22] Raju M, Kumar Khaitan S. Modeling and simulation of compressed air storage in caverns: A case study of the Huntorf plant. Applied Energy. 2012;89:474-81.
[23] Budt M, Wolf D, Span R, Yan J. A review on compressed air energy storage: Basic principles, past milestones and recent developments. Applied Energy. 2016;170:250-68.
[24] Bucker D, Span R, Wagner W. Thermodynamic property models for moist air and combustion gases. Journal of engineering for gas turbines and power. 2003;125:374-84.
[25] Lemmon EW, Jacobsen RT, Penoncello SG, Friend DG. Thermodynamic properties of air and mixtures of nitrogen, argon, and oxygen from 60 to 2000 K at pressures to 2000 MPa. Journal of Physical and Chemical Reference Data. 2000;29:331-85.
[26] Bell IH, Wronski J, Quoilin S, Lemort V. Pure and pseudo-pure fluid thermophysical property evaluation and the open-source thermophysical property library CoolProp. Industrial & engineering chemistry research. 2014;53:2498-508.
[27] Jones AC. Design and test of a small, high pressure ratio radial turbine. ASME 1994 International Gas Turbine and Aeroengine Congress and Exposition: American Society of Mechanical Engineers; 1994. p. V001T01A45-VT01A45.
[28] Crotogino F, Mohmeyer K-U, Scharf R. Huntorf CAES: More than 20 years of successful operation. Orlando, Florida, USA. 2001.
[29] MathWorks I. MATLAB: the language of technical computing. Desktop tools and development environment, version 7: MathWorks; 2005.
[30] Costamagna P, Magistri L, Massardo AF. Design and part-load performance of a hybrid system based on a solid oxide fuel cell reactor and a micro gas turbine. Journal of Power Sources. 2001;96:352-68.